Monthly Notices of the ROYAL ASTRONOMICAL SOCIETY

Mon. Not. R. Astron. Soc. **415,** 3153–3162 (2011) doi:10.1111/j.1365-2966.2011.18928.x

Fermi/GBM and BATSE gamma-ray bursts: comparison of the spectral properties

L. Nava,[1]★ G. Ghirlanda,[2] G. Ghisellini[2] and A. Celotti[1]

[1] *SISSA, via Bonomea 265, I-34136 Trieste, Italy*

[2] *Osservatorio Astronomico di Brera, via E. Bianchi 46, I-23807 Merate, Italy*

Accepted 2011 April 16. Received 2011 March 25; in original form 2011 February 18

ABSTRACT

The Gamma-ray Burst Monitor (GBM) on board *Fermi* allows us to study the spectra of gamma-ray bursts (GRBs) over an unprecedented wide energy range (8 keV–35 MeV). We compare the spectral properties of short and long GRBs detected by the GBM (up to 2010 March) with those of GRBs detected by the Burst And Transient Source Experiment (BATSE) on board the *Compton Gamma Ray Observatory* (*CGRO*). GBM and BATSE long bursts have similar distributions of fluence (F), $E_{\rm peak}^{\rm obs}$ and peak flux (P) but GBM bursts have a slightly harder low-energy spectral index α with respect to BATSE GRBs. GBM and BATSE short bursts have similar distributions of fluence, α and peak flux, with GBM bursts having slightly larger $E_{\rm peak}^{\rm obs}$. We discuss these properties in light of the correlations found between $E_{\rm peak}^{\rm obs}$ and the fluence and the peak flux. GBM bursts confirm that these correlations are not determined by instrumental selection effects. Indeed, GBM bursts extend the $E_{\rm peak}^{\rm obs}$–F and $E_{\rm peak}^{\rm obs}$–P correlations both in fluence/peak flux and in peak energy. No GBM long burst with $E_{\rm peak}^{\rm obs}$ exceeding a few MeV is found, despite the possibility of detecting it. Similarly to what is found with BATSE, there are 3 per cent of GBM long bursts (and almost all short ones) that are outliers at more than 3σ of the $E_{\rm peak}$–$E_{\rm iso}$ correlation. In contrast, there is no outlier of the $E_{\rm peak}$–$L_{\rm iso}$ correlation, for both long and short GBM bursts.

Key words: radiation mechanisms: non-thermal – gamma-ray burst: general.

1 INTRODUCTION

The *Fermi* satellite, launched in 2008 June, offers a great opportunity to characterize gamma-ray burst (GRB) spectra over a wide energy range thanks to its two high-energy instruments: the Large Area Telescope (LAT) and the Gamma-ray Burst Monitor (GBM; Meegan et al. 2009). The GBM is composed of 12 Na I detectors (with good spectral resolution between ∼8 keV and ∼1 MeV) and two BGO detectors (operating between 200 keV and 40 MeV). Significant emission in the LAT energy range (∼30 MeV–300 GeV) has been detected only in about 20 GRBs until now (2010 December), while the GBM detected about 600 GRBs.

A detailed spectral analysis of all GRBs detected by the *Fermi*/GBM up to the end of 2010 March (438 events) has been performed by Nava et al. (2011, hereafter N11). These spectra were fitted with different models and for 318 events (274 long and 44 short) it was possible to constrain the peak energy of the νF_ν spectrum ($E_{\rm peak}^{\rm obs}$). For long bursts we found $\langle E_{\rm peak}^{\rm obs}\rangle \sim 160$ keV and an average low-energy power-law (PL) index $\langle\alpha\rangle \sim -0.9$. Short bursts are found to be harder, in terms of both $E_{\rm peak}^{\rm obs}$ and α: $\langle E_{\rm peak}\rangle \sim$ 490 keV and $\langle\alpha\rangle \sim -0.5$.

N11 also analysed the peak spectrum of GBM bursts, i.e. the spectrum corresponding to the peak flux of the light curve, accumulated on a time-scale of 1.024 and 0.064 s for long and short events, respectively. The comparison with the time-integrated spectral properties shows that peak spectra, on average, have harder low-energy spectral indices but similar peak energies with respect to time-integrated spectra.

Before *Fermi*, other instruments allowed us to study the properties of the prompt emission spectra of GRBs. Due to its broad energy range (∼25 keV to ∼2 MeV), high sensitivity and detection rate, the Burst And Transient Source Experiment (BATSE) on board the *Compton Gamma Ray Observatory (CGRO)* satellite has been so far the instrument best suited to characterizing the GRB prompt emission properties. Thanks to its almost all-sky viewing, BATSE detected more than 2700 GRBs in about 9 years.

The published spectral catalogues of BATSE bursts comprise relatively small sub-samples of *bright* GRBs, selected on the basis of the burst fluence and/or peak flux (Preece et al. 2000; Kaneko et al. 2006, hereafter K06). The analysed samples allowed us to study the spectral properties only of long bursts, given the small number of short bursts present in these samples (e.g. 17 short GRBs in the K06 sample). These studies revealed that the low-energy PL index distribution of long GRBs is centred around $\alpha \sim -1$ and pointed

★E-mail: lara.nava@sissa.it

out the inconsistency of the large majority of burst spectra with a synchrotron interpretation. The $E_{\rm peak}^{\rm obs}$ distribution of long GRBs analysed by K06 peaks around $E_{\rm peak}^{\rm obs} \sim 250$ keV, with a relatively narrow dispersion. However, this refers to bright bursts, while fainter bursts have smaller $E_{\rm peak}^{\rm obs}$ values (Lloyd, Petrosian & Mallozzi 2000; Kippen et al. 2003). Nava et al. (2008, hereafter N08) performed the spectral analysis of a sample of BATSE bursts selected by extending the limiting fluence of K06 (i.e. $F = 2 \times 10^{-5}$ erg cm^{-2}) down to $F = 10^{-6}$ erg cm^{-2}. They found that $E_{\rm peak}^{\rm obs}$ correlates with the fluence F and the peak flux P. This sample of BATSE faint bursts has a distribution of $E_{\rm peak}^{\rm obs}$ values centred at ~150 keV, i.e. a value smaller than the one found for the bright BATSE bursts analysed by K06, as a consequence of the mentioned $E_{\rm peak}^{\rm obs}$–F correlation. This result confirms that the derived distribution of $E_{\rm peak}^{\rm obs}$ is strongly affected by the adopted cuts in fluence (or peak flux).

N08 also found a correlation between $E_{\rm peak}^{\rm obs}$ and the fluence/peak flux for short bursts. This implies that when we compare the $E_{\rm peak}^{\rm obs}$ distributions of short and long GRBs we must take into account the possible different fluence/peak flux selection criteria. A large sample of short BATSE bursts have been analysed by Ghirlanda et al. (2009, hereafter G09). They performed a detailed spectral analysis of 79 short bursts and compared their properties with those of 79 long BATSE bursts selected with the same limit on the peak flux. They found that the $E_{\rm peak}^{\rm obs}$ distributions of the two classes are similar, while the low-energy PL indices are different: short bursts have $\langle\alpha\rangle \sim -0.4$, harder than long events. Their finding of a similar $E_{\rm peak}^{\rm obs}$ distribution for long and short bursts seems to be in contrast with several claims by other authors (Paciesas et al. 2003; Nakar 2007; Guiriec et al. 2010). However, the presence of $E_{\rm peak}^{\rm obs}$–fluence and $E_{\rm peak}^{\rm obs}$–peak flux correlations for long and short events implies that the $E_{\rm peak}^{\rm obs}$ distribution inferred from a given sample of bursts is strongly affected by the criteria adopted to select the sample (often based on the requirement of a minimum peak flux or fluence). The inconsistency between different claims can be easily explained by accounting for the different selection criteria adopted and the different energy ranges of the considered instruments.

A well-known property of long GRBs, related to their prompt emission, is the correlation of the rest-frame peak energy $E_{\rm peak}$ with the bolometric isotropic energy $E_{\rm iso}$ emitted during the prompt (Amati et al. 2002) and with the bolometric isotropic luminosity $L_{\rm p,iso}$ estimated at the peak of the light curve (Yonetoku et al. 2004). Such correlations represent an intriguing clue to the dominant emission mechanism of the prompt phase. Furthermore, if corrected for the jet opening angle, their dispersion reduces considerably (Ghirlanda, Ghisellini & Lazzati 2004a) and allows us to use GRBs as standard candles (Ghirlanda et al. 2004b).

The correlations in the observer frames ($E_{\rm peak}^{\rm obs}$–F and $E_{\rm peak}^{\rm obs}$–P) may be just the consequence of the rest-frame ($E_{\rm peak}$–$E_{\rm iso}$ and $E_{\rm peak}$–$L_{\rm iso}$, respectively) correlations mentioned above. Alternatively, it has been claimed that the rest-frame correlations are the result of instrumental selection effects (Band & Preece 2005; Nakar & Piran 2005). Ghirlanda et al. (2008, hereafter G08) and N08 examined the instrumental selection effects which may affect the observer frame correlations $E_{\rm peak}^{\rm obs}$–F and $E_{\rm peak}^{\rm obs}$–P. They found that, although instrumental biases do affect the burst sample properties, they are not responsible for the correlations found in the observational planes.

Moreover, Ghirlanda, Nava & Ghisellini (2010a) recently showed that the correlations $E_{\rm peak}$–$E_{\rm iso}$ and $E_{\rm peak}$–$L_{\rm p,iso}$ hold for the time-resolved quantities within individual long GBM bursts [see also Firmani et al. (2009) for *Swift* bursts and Krimm et al. (2009) for *Swift–Suzaku* GRBs] and that this 'time–resolved' correlation is similar to that defined by the time-integrated properties of different GRBs. Similar results were found for short GBM bursts: there is a significant correlation between the observer-frame peak energy $E_{\rm peak}^{\rm obs}$ and the peak flux within individual short GRBs, and this correlation has a slope similar to that of the rest-frame $E_{\rm peak}$–$L_{\rm iso}$ correlation (Ghirlanda et al. 2010b). These results confirm that the 'Amati' and 'Yonetoku' correlations have a physical origin, instead of being the result of instrumental selection biases as claimed, and that the trends ($E_{\rm peak}^{\rm obs}$–F and $E_{\rm peak}^{\rm obs}$–P) seen in the 'observational planes' are just their outcome.

Through the spectral catalogue of GBM bursts of N11, we can study the distribution of GBM bursts in the observational planes $E_{\rm peak}^{\rm obs}$–F and $E_{\rm peak}^{\rm obs}$–P and test if the correlations found by BATSE bursts (G08, N08 and G09) still hold. In the observational planes we can also study, for the first time, the possible instrumental biases of GBM for the bursts analysed in N11, and compare the spectral properties of long and short GRBs detected by BATSE and by the GBM. Finally, we can also compute the fraction of GBM short and long GRBs that are outliers, for any assigned redshift, of the rest-frame $E_{\rm peak}$–$E_{\rm iso}$ and $E_{\rm peak}$–$L_{\rm iso}$ correlations. These are the main aims of the present paper.

In Section 2, we present the samples of BATSE and GBM bursts (both long and short) used for our comparison. We compute (Section 3) the relevant instrumental selection effects introduced by the GBM on the observational $E_{\rm peak}^{\rm obs}$–P and $E_{\rm peak}^{\rm obs}$–F planes considering short and long GRBs separately. The comparison between BATSE and GBM results is also presented in terms of spectral parameter distributions in Section 4. We discuss our results and draw our conclusions in Section 5.

2 SAMPLES

2.1 Long bursts

2.1.1 BATSE

Fig. 1 shows the $\log N$–$\log F$ of long GRBs detected by BATSE (open squares), where N is the number of objects with fluence

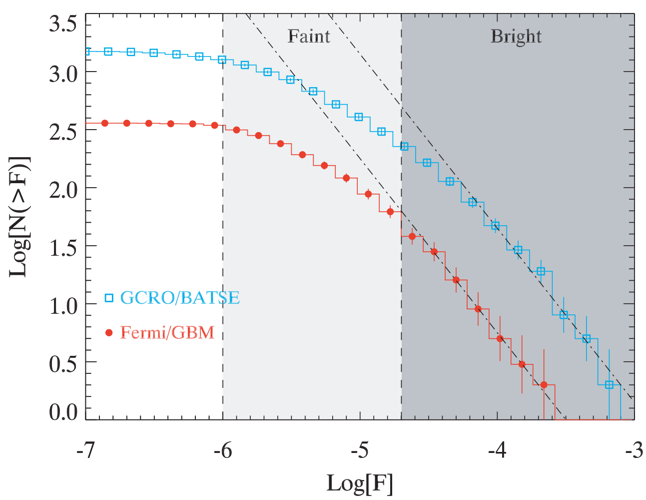

Figure 1. Long GRBs. Log N–log F for long BATSE bursts (empty squares) and long GBM bursts (filled circles). In both cases, the fluence F is integrated between 20 and 2000 keV. GBM data are taken from N11, while BATSE data are from the online catalogue and include all the BATSE bursts for which the fluence has been estimated. For reference two PLs with slope −3/2 are shown (dot–dashed lines).

larger than F. Since we compare this $\log N$–$\log F$ with that of GBM bursts (filled squares in Fig. 1), we compute F in the energy range between 20 and 2000 keV, which is common to both instruments. BATSE fluences are taken from the online *CGRO*/BATSE Gamma-ray Bursts Catalogue.[1]

We have then considered the spectral catalogue of K06 which contains all BATSE bursts with peak flux $P(50\text{–}300\,\text{keV}) > 10\,\text{photons cm}^{-2}\,\text{s}^{-1}$ *or* fluence $F(20\text{–}2000\ \text{keV}) > 2 \times 10^{-5}$ erg cm^{-2}. From the 350 events of this sample we extract the long ones, i.e. with observed duration $T_{90} > 2$ s. Among these, 280 GRBs have a well-determined $E^{\rm obs}_{\rm peak}$ (i.e. their spectra are best fitted by a curved model with $\alpha < -2$ or $\beta > -2$, i.e. showing a peak in a νF_ν representation). For 104 events the spectrum is best fitted by a Band model (Band et al. 1993), for 65 by a Comptonized (COMP) model [a PL with a high-energy exponential cut-off] and for 111 by a smoothly broken power-law (SBPL) model.

Although the K06 analysis enlarges the previous spectral catalogue of BATSE bursts (Preece et al. 2000), it still selects only the brightest BATSE bursts (i.e. corresponding to only 13 per cent of the entire population of bursts detected by BATSE). N08 selected a sample of 100 BATSE bursts with a fluence fainter than the threshold adopted by K06. The N08 events, in fact, have a fluence in the range $10^{-6} < F < 2 \times 10^{-5}$ erg cm^{-2}. Moreover, although these are only 100 bursts, they are representative of the large population of ∼1000 bursts in this fluence range since they were randomly extracted following the $\log N$–$\log F$ distribution of BATSE GRBs in this fluence range. Of these 100 representative bursts, 44 are best fitted by the COMP model, 44 by the Band model and 12 by a PL function. Therefore, the N08 sample contains 88 GRBs with a spectrum fitted by a curved model, for which $E^{\rm obs}_{\rm peak}$ was well determined. Among the bursts analysed by K06 with peak flux P larger than 10 photons cm^{-2} s^{-1}, there are GRBs with fluences smaller than $F = 2 \times 10^{-5}$ erg cm^{-2} that overlap with the ones studied by N08. We exclude these bursts from the present discussion in order to have well-defined complete samples at two limiting fluences that we will call, in the rest of the paper, the 'bright' BATSE bursts (the bursts in K06 with $F > 2 \times 10^{-5}$ erg cm^{-2}) and the 'faint' BATSE bursts (the bursts studied in N08 with $10^{-6} < F < 2 \times 10^{-5}$ erg cm^{-2}). The grey shaded regions in Fig. 1 correspond to this sub-division.

2.1.2 *GBM*

In N11, we have analysed the spectra of all the GRBs detected by the GBM up to 2010 March (438 GRBs). No fluence or peak flux selection has been adopted. Fig. 1 shows that the shape of $\log N$–$\log F$ for the two instruments is very similar. To compare the $E^{\rm obs}_{\rm peak}$ and α distribution of GBM bursts with those of BATSE bursts, we select from the N11 catalogue two subsamples with the same fluence criterion adopted by K06 and N08 for BATSE bursts, and we call them the *bright GBM sample* and the *faint GBM sample*.

In six GBM bursts, N11 could not analyse the spectrum, due to lack of data. For the remaining 432 bursts we performed the spectral analysis using a PL model (109 spectra), a COMP model (258 spectra) and a Band model (65 spectra) and evaluating for each burst the spectral parameters of the best-fitting model. 359 events belong to the long burst class. We also estimated their peak flux on a time bin of 1.024 s. In this work we will use this sample of GBM long bursts for comparison with BATSE long GRBs.

[1] http://heasarc.gsfc.nasa.gov/W3Browse/cgro/batsegrb.html

2.2 Short bursts

2.2.1 *BATSE*

The most comprehensive sample of short BATSE GRBs with well-defined spectral parameters is composed of the 79 events analysed by G09, selected for having $P > 3\,\text{photons cm}^{-2}\,\text{s}^{-1}$. In 71 cases the spectra have a well-determined $E^{\rm obs}_{\rm peak}$.

2.2.2 *GBM*

For the GBM instrument we use the spectral parameters of the 44 short GRBs present among the 438 bursts analysed by N11 with a well-determined $E^{\rm obs}_{\rm peak}$. Their peak flux is estimated on a time bin of 0.064 s.

3 $E^{\rm obs}_{\rm peak}$–FLUENCE AND $E^{\rm obs}_{\rm peak}$–PEAK FLUX PLANES: COMPARISON BETWEEN BATSE AND GBM BURSTS

A correlation between the total fluence and $E^{\rm obs}_{\rm peak}$ was first found by Lloyd et al. (2000) for a sample of BATSE bursts without measured redshifts. This finding was recently confirmed by Sakamoto, Hullinger & Sato (2008) using a sample of bursts detected by *Swift*, BATSE and *Hete-II*. In particular, they noted that X-ray flashes and X-ray rich bursts satisfy and extend this correlation to lower fluences. A similar result was found by Kippen at al. (2003), who noted that X-ray flashes extend the $E^{\rm obs}_{\rm peak}$–P correlation.

The distribution of GRBs with and without measured redshift in the planes $E^{\rm obs}_{\rm peak}$–F and $E^{\rm obs}_{\rm peak}$–P has been investigated by G08 and N08. N08 considered all events with published spectral information detected by different instruments (*Swift*, BATSE, *Hete-II*, Konus/Wind and *Beppo*SAX) together with the 100 faint BATSE bursts analysed in that paper. In both planes long bursts define a correlation, with fainter bursts having lower $E^{\rm obs}_{\rm peak}$.

In order to examine the distribution of GBM bursts in the observational planes $E^{\rm obs}_{\rm peak}$–F and $E^{\rm obs}_{\rm peak}$–P and compare it with the BATSE bursts we have to first estimate the possible instrumental biases induced by the detector (see G08). One instrumental bias is the capability of an instrument to be triggered by a burst, i.e. the 'trigger threshold' (TT) [first computed by Band (2003) for different detectors]. The second bias concerns the minimum number of photons required to analyse the spectrum and constrain the spectral parameters. This is called the 'spectral threshold' (ST) in G08 and N08. The TT translates into a minimum peak flux, which depends on the burst spectrum and in particular on its $E^{\rm obs}_{\rm peak}$ and can be described as a curve in the $E^{\rm obs}_{\rm peak}$–P plane. The second requirement (ST) results in a minimum fluence which depends on $E^{\rm obs}_{\rm peak}$ and also on the burst duration. For this reason the ST is represented as a region (i.e. not a line) in the $E^{\rm obs}_{\rm peak}$–F plane.

These curves (TT and ST) divide the observational planes $E^{\rm obs}_{\rm peak}$–F and $E^{\rm obs}_{\rm peak}$–P into two regions. Bursts with peak energy and peak flux that place them on the left of the TT curve cannot be triggered by the corresponding instrument. Similarly, bursts with peak energy and fluence that place them on the left side of the ST curves do not have enough photons to allow a reliable spectral analysis (see G08 for more details).

3.1 Estimate of GBM instrumental selection effects

Following G08, the TT curves are obtained adapting the results of Band (2006) and are shown in the right (top and bottom) panels of

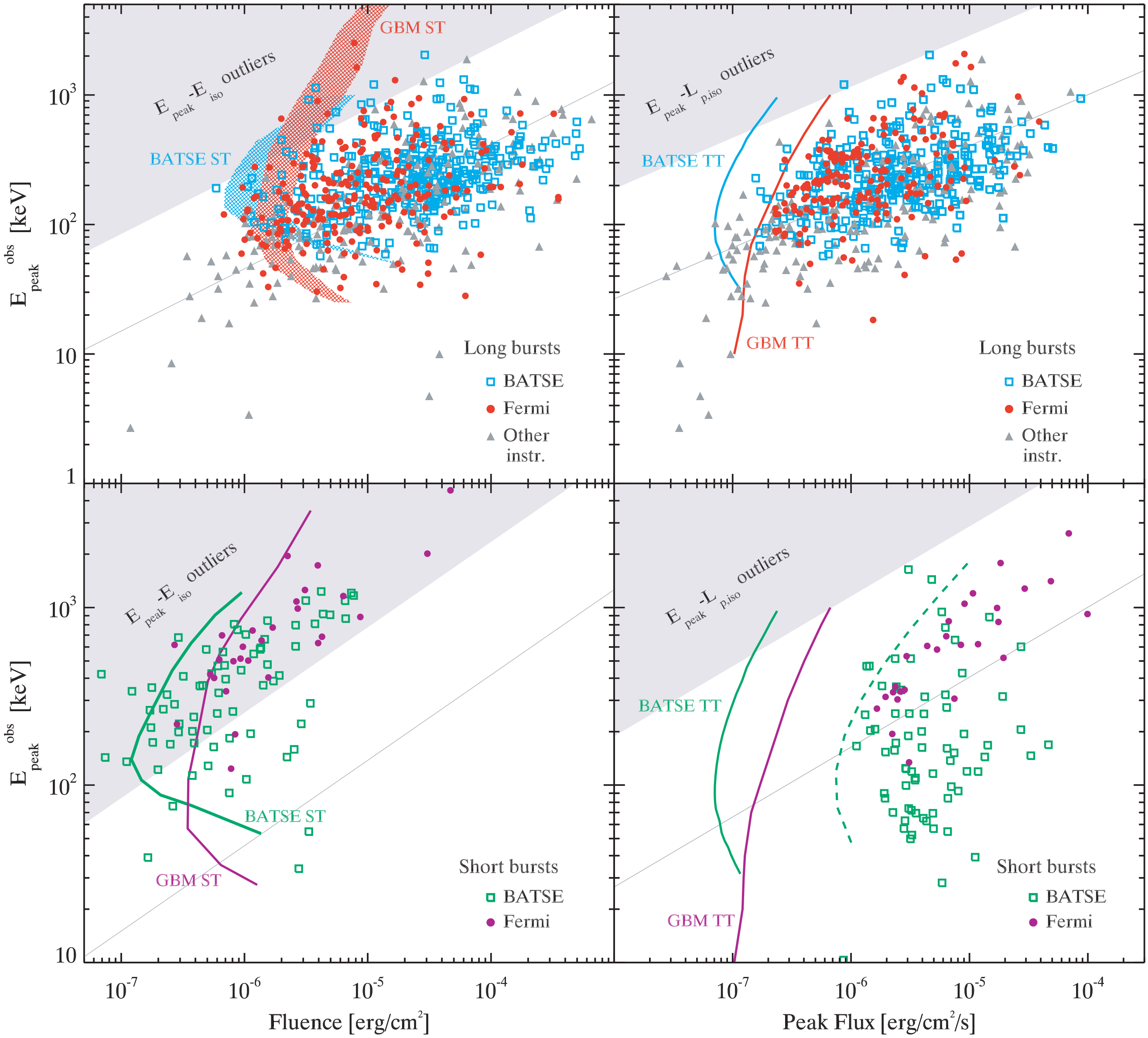

Figure 2. $E_{\rm peak}^{\rm obs}$–fluence and $E_{\rm peak}^{\rm obs}$–peak flux planes for long (upper panels) and short (bottom panels) bursts. Empty squares represent BATSE bursts, filled circles represent GBM bursts and filled triangles indicate events detected by other instruments (from N08). In all panels the instrumental limits for BATSE and GMB are reported: shaded curved regions in the upper-left panel show the ST, estimated assuming a burst duration of 5 and 20 s; solid curves in the bottom-left panel represent the ST for short bursts. Solid curves in the right-hand panels define the TT, identical for short and long events. Thresholds for BATSE are taken from G08 while those for the GBM instrument are derived in this work (see Section 3.1). The dashed curve in the bottom-right panel represents the selection criterion applied by G09 for their sample of short bursts, i.e. $P > 3$ photons cm^{-2} s^{-1}. The shaded regions in the upper-left corners of all the planes are the region identifying the outliers at more than 3σ of the $E_{\rm peak}$–$E_{\rm iso}$ (left-hand panels) and $E_{\rm peak}$–$L_{\rm iso}$ (right-hand panels) correlations for any given redshift. GRBs, without measured redshift, which fall in these regions are outliers of the corresponding rest-frame correlations ($E_{\rm peak}$–$E_{\rm iso}$ and $E_{\rm peak}$–$L_{\rm iso}$ for the left- and right-hand panels, respectively) for any assigned redshift. It means that there is no redshift which makes them consistent with these correlations (considering their 3σ scatter).

Fig. 2. The TT curves are the same for long and short bursts as the TT depends only on the peak flux.

The ST curves have been calculated from numerical simulations, as described in G08. To perform these simulations, the typical background spectrum and the detector response function are required. For the bursts detected by the GBM both of them depend on several factors (e.g. the satellite attitude when a burst occurs), and thus there is no universal background and response matrix which can be adopted. To overcome this problem we use the real backgrounds and responses of several GRBs detected by the GBM and average the results of the simulations to build average ST curves for the population of long and short bursts, respectively.

Our simulation performs a joint spectral analysis of spectra simulated for two Na I detectors and one BGO detector. For long bursts, simulations were performed using the detector response files and the background spectra of the long GBM bursts published in G10. We considered, as done in G08, two representative values of the duration, i.e. $T_{90} = 5$ and 20 s (corresponding in Fig. 2 to the curves delimiting the red shaded region on the left- and right-hand sides, respectively). For short bursts we estimated the ST curves adopting the response files and the background spectra of the short bursts of the GBM sample of N11 assuming a typical duration of the simulated spectra of 0.7 s (red curve in the bottom-left panel of Fig. 2). This value, also adopted by G08 for BATSE bursts, corresponds to the typical duration of short GRBs observed by the GBM.

For the TT and ST curves of the BATSE instrument we simply report those obtained in G08 (for long bursts) and in G09 (for short bursts).

Fig. 2 shows the distribution of GBM bursts in the $E^{\rm obs}_{\rm peak}$–F and $E^{\rm obs}_{\rm peak}$–P planes (right and left panels) for long and short GRBs (upper and bottom panels).

3.1.1 Long bursts

$E^{\rm obs}_{\rm peak}$ *versus fluence.* As can be seen in the top-left panel of Fig. 2, the distribution of long GBM bursts (filled circles) extends down to the lower end of the distribution of BATSE bursts (empty squares).

The presence of GBM bursts with low $E^{\rm obs}_{\rm peak}$ (between $\sim$10 and $\sim$50 keV), not present in the BATSE sample, is clearly due to the wider energy range of the GBM instrument, sensitive down to $\sim$8 keV (see the ST curves). In this region, GBM bursts are consistent with bursts detected by other instruments (filled triangles). We also note that GBM bursts define a correlation which mostly overlaps with that defined by BATSE bursts and extends to the lower-left part of the $E^{\rm obs}_{\rm peak}$–F plane.

Despite the fact that the GBM assures good coverage up to $\sim$30 MeV (versus $\sim$1 MeV of BATSE), there are only a few long GRBs with $E^{\rm obs}_{\rm peak}$ exceeding a few MeV, similar to what is found for the population of BATSE bursts. Note that high $E^{\rm obs}_{\rm peak}$ also means GRBs with high fluences, which are rarer than GRBs with low fluences.

Note also that while BATSE bursts appear concentrated at the high end of the $E^{\rm obs}_{\rm peak}$–F correlation, the sample is composed of *all* bursts with $F > 2 \times 10^{-5}$ erg cm^{-2} (the K06 sample) and only *one hundred* fainter bursts (the N08 sample) representative of $\sim$1000 objects with $10^{-6} < F < 2 \times 10^{-5}$ erg cm^{-2}. Therefore, the real density of BATSE bursts in the latter fluence range is much larger than that represented in Fig. 2 (see e.g. fig. 8 in N08) so that the slight shift between BATSE and GBM population density in the upper panels is only an apparent effect.

Another result shown by the GBM bursts and consistent with the conclusion drawn from BATSE is that the ST effect is not responsible for the distribution of the data in the plane, i.e. it cannot explain why bursts tend to distribute along a correlation. This is well visible for BATSE bursts: events with large $E^{\rm obs}_{\rm peak}$ tend to concentrate far from the ST, i.e. at higher fluences. The trend shown by the BATSE ST (which requires higher limiting fluences when $E^{\rm obs}_{\rm peak}$ is very high and very low) cannot explain this behaviour. The same holds for GBM bursts, for which the ST are even less curved and cannot be responsible for the observed correlation which has a slope $\sim$0.20 $\pm$ 0.04, consistent with that defined by BATSE bursts (N08).

$E^{\rm obs}_{\rm peak}$ *versus peak flux.* The distribution of GBM long bursts in the $E^{\rm obs}_{\rm peak}$–P plane with respect to BATSE bursts is shown in the upper-right panel of Fig. 2. Solid curves represent the TT derived for both instruments (adapted from Band 2006). On average, the GBM instrument is a factor of 3 less sensitive than BATSE in the common energy range. As remarked by N08, the sample of BATSE bursts lies far from its TT, suggesting that for this instrument the demand of performing a reliable spectral analysis is the dominant selection query. This is not the case for the GBM: the data points lie very near the TT curves, suggesting that if a burst is detected there is a good chance to recover its spectral parameters. This makes TT and ST competitive selection effects for GBM bursts.

3.1.2 Short bursts

For short bursts (bottom panels in Fig. 2) the situation is quite different in both $E^{\rm obs}_{\rm peak}$–F and $E^{\rm obs}_{\rm peak}$–P planes than for long events.

Although GBM short bursts are still only a few (filled circles in Fig. 2) there is a weak indication of a correlation in both planes (left and right bottom panels in Fig. 2), consistent with the trends suggested by BATSE short bursts (open squares). However, the overall behaviour is different from what happens for long GRBs.

At high $E^{\rm obs}_{\rm peak}$ GBM short events occupy the same region as the BATSE ones, and even extend the $E^{\rm obs}_{\rm peak}$–F trend to $E^{\rm obs}_{\rm peak}$ values larger than 1 MeV (i.e. above the BATSE upper threshold), revealing that short GRBs with $E^{\rm obs}_{\rm peak}$ larger than 1 MeV exist in the population of GBM events.

Furthermore, contrary to what one might expect, there are no short GBM bursts with $E^{\rm obs}_{\rm peak}$ below $\sim$200 keV. At low fluences this can be accounted for by considering the ST derived for the GBM instrument: Fig. 2 shows that GBM short events lie very near to the ST curve (bottom-left panel of Fig. 2), which prevents the estimate of $E^{\rm obs}_{\rm peak} < 200$ keV when $F < 4 \times 10^{-7}$ erg cm^{-2}.

The higher sensitivity of BATSE instead implies that its ST is located at lower fluences. This, however, does not account for the absence of short GBM bursts with $E^{\rm obs}_{\rm peak} < 200$ keV and fluence $>5 \times 10^{-7}$ erg cm^{-2}: the BATSE sample shows that GRBs with low $E^{\rm obs}_{\rm peak}$ but on the right side of the GBM ST do exist. Their absence in the present GBM sample seems to imply that they are relatively rare and that the still small size of the present sample of GBM short bursts prevents us from observing these events. The rarity of these objects supports the existence of an $E^{\rm obs}_{\rm peak}$–F correlation for short GRBs: at a fluence $>4 \times 10^{-7}$ erg cm^{-2} most of the events should have $E^{\rm obs}_{\rm peak} > 200$ keV. A larger sample of short GBM bursts is required to confirm this.

In terms of $E^{\rm obs}_{\rm peak}$ this translates into a distribution peaked at higher energies compared both to the BATSE one and to the GBM long events (see Section 4.2).

In the $E^{\rm obs}_{\rm peak}$–P plane of short GRBs (right-bottom panel in Fig. 2) similar conclusions can be drawn: for both instruments the TT curves (solid lines) do not affect the samples. Both samples are clearly limited by the selection cut applied on the peak flux (shaded curve). From the fact that the peak flux of GBM bursts is significantly above their TT, we infer that their selection is dominated by the ST.

3.2 Outliers of the $E_{\rm peak}$–$E_{\rm iso}$ and $E_{\rm peak}$–$L_{\rm iso}$ correlations

Another relevant point is to test whether bursts without measured redshifts are consistent with the $E_{\rm peak}$–$E_{\rm iso}$ and $E_{\rm peak}$–$L_{\rm iso}$ correlations. These correlations are defined in the rest frame and require, to add a burst on top of them, to have the redshift known. However, as first proposed by Nakar & Piran (2005) and then by Band & Preece (2005), knowing $E^{\rm obs}_{\rm peak}$ and the fluence or peak flux it is still possible to test if a burst, without measured redshift, is an outlier of the $E_{\rm peak}$–$E_{\rm iso}$ and $E_{\rm peak}$–$L_{\rm iso}$ correlations.

In the observational planes, it is possible to define a 'region of outliers'. We start by writing the $E_{\rm peak}$–$E_{\rm iso}$ correlation as (the same argument can be repeated for the $E_{\rm peak}$–$L_{\rm iso}$ correlation)

$$E_{\rm peak} = K E^{\eta}_{\rm iso}. \qquad (1)$$

Since $E_{\rm peak}^{\rm obs} = E_{\rm peak}/(1+z)$ and $F = E_{\rm iso}(1+z)/4\pi d_L^2(z)$, we can form the ratio

$$\frac{(E_{\rm peak}^{\rm obs})^{1/\eta}}{F} = K^{1/\eta}\, 10^{\pm\sigma/\eta}\, \frac{4\pi d_L^2(z)}{(1+z)^{(1+\eta)/\eta}}, \qquad (2)$$

where σ corresponds to the scatter of data points around the rest-frame correlation that is being tested. *Note that this is not the error on the slope or normalization of the correlation, but the scatter measured perpendicular to the best-fitting line of the $E_{\rm peak}$–$E_{\rm iso}$ correlation and modelled as a Gaussian distribution.*

The RHS of the above relation is a function of z, η and σ only. The upper limit of the ratio $E_{\rm peak,obs}^{1/\eta}/F$ establishes an allowance region boundary on the corresponding plane (upper-left-corner shaded regions in Fig. 2). All the bursts that fall below this line in the observational planes can have a redshift which makes them consistent with the $E_{\rm peak}$–$E_{\rm iso}$ correlation within its 3σ scatter. Those falling in the shaded region are outliers at more than 3σ for any assigned redshift.

Although this test has been already applied several times in the recent past, some guidelines should be followed.

(i) Since the rest-frame correlations are defined with the bolometric 1 keV–10 MeV $E_{\rm iso}$ and $L_{\rm p,iso}$, when testing the region of outliers in the observational planes one should use the fluence F and peak flux P defined on the same energy range.

(ii) It is correct to consider the 3σ scatter of the rest-frame correlations and not the uncertainty on the slope (η) and normalization (K) of the correlations. This is because the scatter σ of the $E_{\rm peak}$–$E_{\rm iso}$ and $E_{\rm peak}$–$L_{\rm iso}$ correlations dominates over the statistical uncertainty on K and η (e.g. G10).

(iii) While the $E_{\rm peak}$–$E_{\rm iso}$ and $E_{\rm peak}$–$L_{\rm iso}$ correlations were first derived with only a dozen bursts, they have now been updated with nearly 100 GRBs with measured redshifts (e.g. N08, G10): the correlation parameters (slope, normalization and scatter) have changed since their discovery, so one should adopt the most updated versions of these correlations.

N08 find that 6 per cent of BATSE long bursts are outliers of the $E_{\rm peak}$–$E_{\rm iso}$ correlation, while no outlier is found for the $E_{\rm peak}$–$L_{\rm p,iso}$ correlation. Almost all short BATSE bursts are outliers of the $E_{\rm peak}$–$E_{\rm iso}$ correlation (defined by long bursts) but they can be consistent with their very same $E_{\rm peak}$–$L_{\rm p,iso}$ correlation. These findings are supported by the consistency of the few short bursts with measured redshift with the $E_{\rm peak}$–$L_{\rm iso}$ correlation while they are outliers at more than 3σ of the $E_{\rm peak}$–$E_{\rm iso}$ correlation (G09).

For GBM long bursts, Fig. 2 shows that eight GRBs (i.e. 3 per cent) lie in the region of outliers (in the $E_{\rm peak}^{\rm obs}$–F plane), even if the extended energy range of the GBM allows us to explore the region of large $E_{\rm peak}^{\rm obs}$ and intermediate fluences, where outliers, if they exist, could be found. The percentage of outliers that we find is larger than 0.3 per cent (which is the expected number if we assume that the correlation has a perfect Gaussian scatter). This implies that the true $E_{\rm peak}$–$E_{\rm iso}$ correlation is somewhat different (i.e. larger) from that presently defined by the sample of 105 GRBs with measured redshift and/or that a Gaussian distribution is not the best way to describe its scatter.

For short GBM bursts, we can see that most of them are outliers at more than 3σ of the $E_{\rm peak}$–$E_{\rm iso}$ correlation. In contrast, there are no short bursts in the region of outliers in the $E_{\rm peak}^{\rm obs}$–P plane, i.e. they are all consistent with the $E_{\rm peak}$–$L_{\rm iso}$ correlation defined by long GRBs. The hypothesis that short and long bursts follow the same $E_{\rm peak}$–$L_{\rm p,iso}$ correlation is also supported by the few short events with known redshift (G09).

4 SPECTRAL PARAMETER DISTRIBUTIONS

In this section we compare the distributions of the spectral parameters (low-energy spectral index α and peak energy $E_{\rm peak}^{\rm obs}$) for long (Section 4.1) and short (Section 4.2) GRBs detected by BATSE and by the GBM. In addition, we show the log N–log P distribution for short bursts.

4.1 Long bursts

Fig. 3 (upper panel) shows the distributions of $E_{\rm peak}^{\rm obs}$ of bright BATSE and bright GBM bursts. The two distributions are quite similar: the central value of the Gaussian fit (solid line) is $E_{\rm peak}^{\rm obs} \sim 260$ keV and $E_{\rm peak}^{\rm obs} \sim 280$ keV, respectively, with GBM bursts having a larger distribution (standard deviation $\sigma = 0.33$ to be compared with $\sigma = 0.21$ for BATSE bursts) and extending both at lower and at higher $E_{\rm peak}^{\rm obs}$ with respect to that of BATSE. Using the Kolmogorov–Smirnov (KS) test, we find that the probability that the two distributions are drawn from the same parent population is 0.073.

For faint bursts (bottom panel of Fig. 3) the results are similar. For both instruments the Gaussian fit to the $E_{\rm peak}^{\rm obs}$ distribution is centred around 140 keV and has a standard deviation $\sigma \sim 0.30$ (the

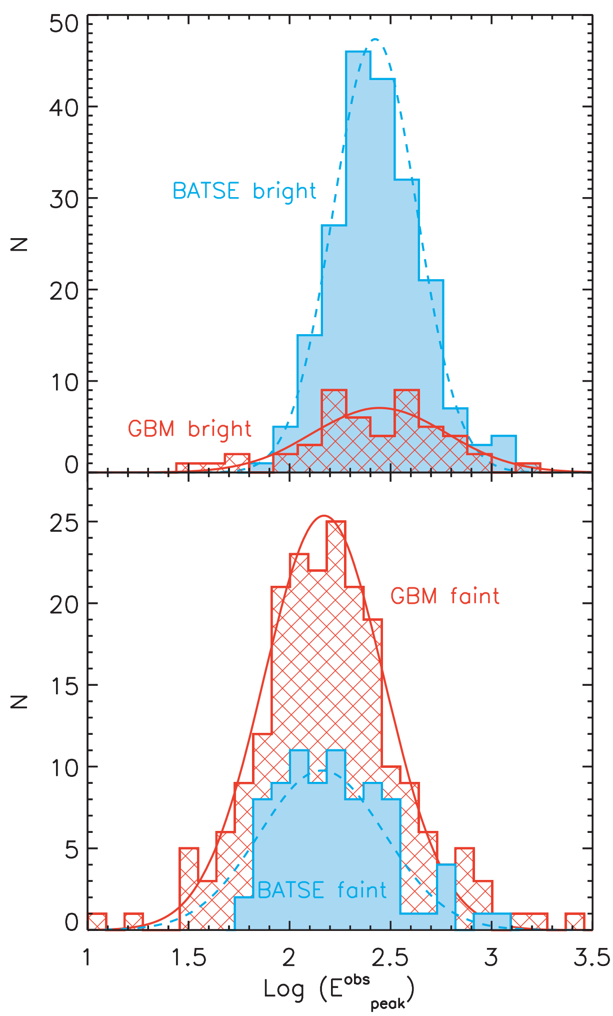

Figure 3. Long GRBs. $E_{\rm peak}^{\rm obs}$ distribution for BATSE bursts (blue solid filled histograms) and GBM bursts (red hatched histograms). For both instruments, we separately plot the $E_{\rm peak}^{\rm obs}$ distributions for the bright sample (upper panel) and the faint sample (bottom panel).

Table 1. Central values and standard deviations (in brackets) of the distributions of α and $E_{\rm peak}^{\rm obs}$ for long and short bursts. The table also lists the KS probability resulting from the comparison between BATSE and GBM distributions of α and $E_{\rm peak}^{\rm obs}$. For long bright bursts the comparison has been done by considering (for homogeneity) bursts best modelled by a COMP or a Band model (i.e. by excluding from K06 those bursts modelled with an SBPL model).

Parameter	Long						Short		
	Bright			Faint					
	BATSE	*Fermi*	KS	BATSE	*Fermi*	KS	BATSE	*Fermi*	KS
$E_{\rm peak}$	2.42 (0.21)	2.45 (0.33)	0.073	2.16 (0.31)	2.17 (0.30)	0.387	2.60 (0.42)	2.79 (0.27)	1.1×10^{-3}
α	−1.00 (0.31)	−0.95 (0.23)	0.462	−1.02 (0.57)	−0.93 (0.36)	0.116	−0.40 (0.50)	−0.59 (0.11)	0.018

KS test probability is 0.387). Also in this case the GBM distribution is larger. In particular, from the comparison of the two histograms it appears that GBM data allow us to recover very low $E_{\rm peak}^{\rm obs}$, thanks to the good GBM/Na I sensitivity down to 8 keV (i.e. extending by a factor of 3 the low-energy bound of BATSE). For BATSE bursts, there is a quite sharp cut-off at ~ 50 keV. This is in agreement with the simulations performed by G08 (see Fig. 2) showing that it is very difficult for BATSE to recover $E_{\rm peak}^{\rm obs} < 50$ keV. Large fluences, unusual for such values of $E_{\rm peak}^{\rm obs}$, would be required. All the results of the Gaussian fits and KS probabilities are summarized in Table 1.

We stress that the $E_{\rm peak}^{\rm obs}$ properties of faint and bright bursts are very different due to the correlation between $E_{\rm peak}^{\rm obs}$ and F: the faint sample is characterized by a central value of $E_{\rm peak}^{\rm obs}$ which is almost a factor of 2 lower than that of the bright sample. The KS probability of the distributions of $E_{\rm peak}^{\rm obs}$ within the GBM sample between faint and bright bursts is 8×10^{-5}.

Fig. 4 shows the α distribution for bright (upper panel) and faint bursts (bottom panel). In both cases, GBM bursts tend to have a harder low-energy PL index and a somewhat tighter distribution (central values and standard deviations of the Gaussian fits are reported in Table 1). However, the KS test shows that the α distributions of faint GBM and faint BATSE bursts are similar (KS probability = 0.116). Moreover, GBM bursts do not show a significant relation between α and the fluence because faint and bright GBM bursts have similar distributions peaked, respectively, at −0.93 and −0.95 and with a KS probability of 0.21.

The α distribution of bright BATSE bursts (grey histogram), instead, shows a significant difference with respect to both the bright GBM sample (KS probability $= 7 \times 10^{-3}$) and the faint BATSE sample (KS probability $= 7 \times 10^{-3}$). Bright BATSE bursts tend to have softer α with respect to all the other samples. We investigated the possible origin of this difference considering that the K06 sample contains bursts whose spectra are fitted with the SBPL, COMP or Band model. As noted by K06 themselves the spectral parameters $E_{\rm peak}^{\rm obs}$ and α do show different typical values and widths of their distributions depending on the fitting spectral model. Considering that GBM bursts are adequately fitted by either the COMP or the Band model, we excluded from the $E_{\rm peak}^{\rm obs}$ distribution of BATSE bursts the bursts fitted with an SBPL model. The resulting histogram (dark blue shaded in Fig. 4) is now fully consistent with the distribution of α of GBM bursts (the KS probability now becomes 0.46).

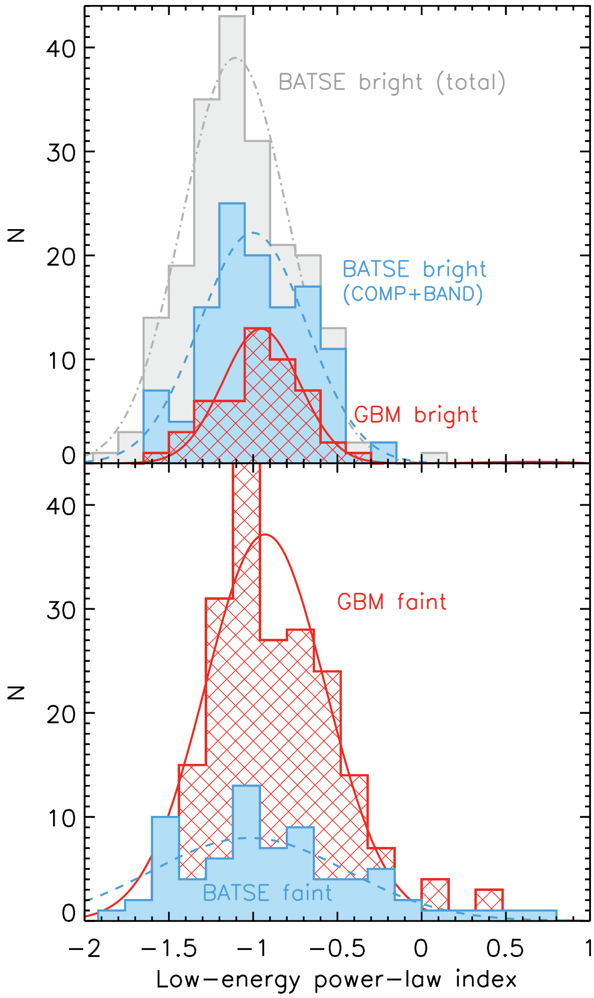

Figure 4. Long GRBs. Low-energy PL index α distributions for BATSE bursts (blue solid filled histograms) and GBM bursts (red hatched histogram). For both instruments, we separately plot the distributions for the bright sample (upper panel) and the faint sample (bottom panel). For the bright BATSE sample of K06 (upper panel) we also show separately the α distribution of bursts fitted with all models (light grey shaded histogram) and that of bursts fitted with only the COMP or Band model (grey histogram).

4.2 Short bursts

The largest sample of BATSE bursts for which the spectral analysis has been performed was selected on the basis of a peak flux criterion (G09). A meaningful comparison between GBM and BATSE short bursts requires a sample of short GBM bursts selected on the basis of the very same criterion. Before investigating the spectral parameter distributions, we compare the $\log N$–$\log P$ for both instruments,

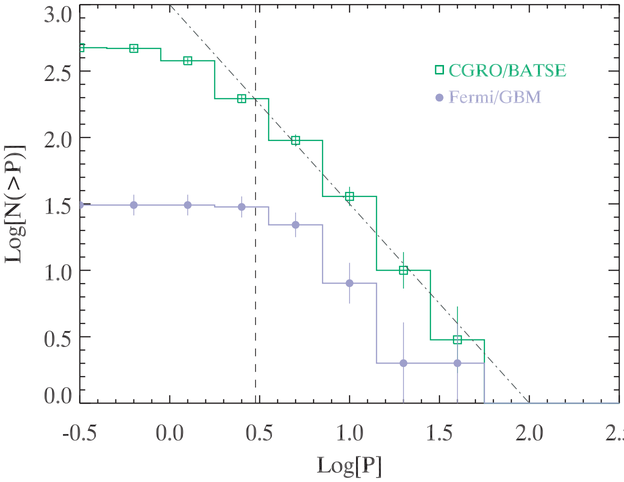

Figure 5. Short GRBs. Log N–log P for short BATSE bursts (empty squares) and short GBM bursts (filled circles). In both cases, the peak flux P (in photons cm^{-2} s^{-1}) is integrated between 50 and 300 keV on a time-scale of 64 ms. GBM data are taken from N11, while BATSE data are from the online catalogue and include all the BATSE bursts for which the peak flux has been estimated. The vertical dashed line is the flux limit of the selection of BATSE bursts analysed in G09 and for reference a PL with slope –3/2 is shown (dot–dashed line).

where P in this case is the peak flux in photons cm^{-2} s^{-1}. Since for the GBM sample N11 estimate the peak flux on a 64 ms time-scale, also for BATSE bursts we select (from the online catalogue[2]) all bursts for which P on a 64 ms time-scale has been estimated. For BATSE bursts the peak flux is integrated in the 50–300 keV energy range. Therefore, we estimate for all short GBM bursts in N11 the photon peak flux between 50 and 300 keV. Fig. 5 shows our results.

As discussed in Section 3 the lack of bursts with low peak flux in the GBM sample is due to the ST threshold shown in Fig. 2. This instrumental threshold, indeed, dominates over the TT threshold and determines that short GRBs for which the spectrum can be analysed and the spectral parameters properly constrained should have a large number of photons. At high peak fluxes instead, GBM has detected more short GRBs than BATSE due to the $E_{\rm peak}^{\rm obs}$–P correlation, which associates high peak fluxes with high peak energies, the latter better constrained with the larger energy range of the GBM instrument (BGO) than with BATSE. This explains the different shapes of the two log N–log P.

To compare the spectral parameters, we consider short GRBs (from G09 for BATSE and N11 for GBM) with known α and $E_{\rm peak}^{\rm obs}$ and with $P(50–300\,{\rm keV}) > 3$ photons cm^{-2} s^{-1}. The $E_{\rm peak}^{\rm obs}$ distributions are shown in Fig. 6 and are quite different. The lack of low $E_{\rm peak}^{\rm obs}$ in the GBM sample (which corresponds to the lack of low peak fluxes in Fig. 6) can be explained by considering the shape and position of the ST for short bursts (left-bottom panel in Fig. 2), the existence of a correlation between P and $E_{\rm peak}^{\rm obs}$, and the small size of the present sample of GBM short GRBs (see the above discussion and Section 2). Moreover, contrary to long bursts, the $E_{\rm peak}^{\rm obs}$ distribution of GBM short events extends to higher energies, suggesting that such large values of $E_{\rm peak}^{\rm obs}$ can be found in short bursts and that they were not present in the BATSE catalogue due to its limited energy range (up to only $\sim$ 1 MeV).

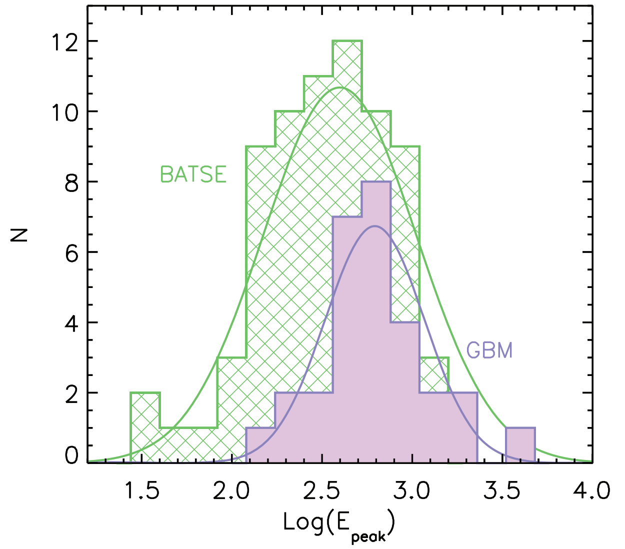

Figure 6. Short GRBs. $E_{\rm peak}^{\rm obs}$ distribution for BATSE bursts (green hatched histogram, from G09), and GBM bursts (purple filled histogram, from N11).

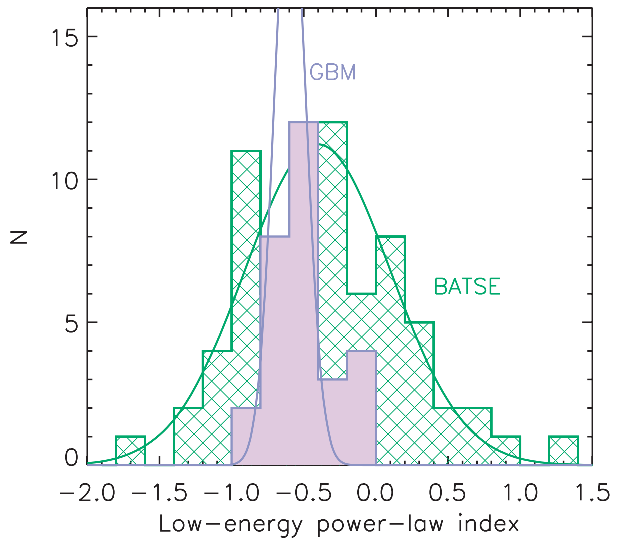

Figure 7. Short GRBs. α distribution for BATSE bursts (green hatched histogram, from G09) and GBM bursts (purple filled histogram, from N11).

The α distributions of BATSE and GBM bursts (Fig. 7) are considerably different. The GBM confirms that short events are harder than long ones in terms of the low-energy spectral index (KS probability $= 3 \times 10^{-8}$). However, the distribution is peaked around $\alpha = -0.59$ and it is very narrow ($\sigma = 0.11$). We tentatively interpret this as due to the large energy range of GBM which extends down to 8 keV, but this point deserves further study. The extension down to low energies of GBM allows us in principle to determine α more accurately. Instead, the limited energy range of BATSE resulted in less accurate estimates of α and thus a more dispersed distribution of its values. This effect is slightly present also in long bursts, both bright and faint (see Table 1).

5 DISCUSSION AND CONCLUSIONS

In this work we have investigated the presence of the $E_{\rm peak}^{\rm obs}$–fluence and $E_{\rm peak}^{\rm obs}$–peak flux correlations in GBM bursts (both long and

[2] http://heasarc.gsfc.nasa.gov/W3Browse/cgro/batsegrb.html

short) detected by the GBM instrument up to 2010 March. Similarly to what has been done for long and short GRBs detected by BATSE (N08; G09) we examined the distribution of GBM bursts in the $E_{\rm peak}^{\rm obs}$–fluence and $E_{\rm peak}^{\rm obs}$–peak flux planes in order to study instrumental selection effects and test their consistency with the rest-frame correlations (i.e. $E_{\rm peak}$–$E_{\rm iso}$ and $E_{\rm peak}$–$L_{\rm iso}$, respectively) defined by GRBs with measured redshifts. To this aim, we have estimated, for the GBM instrument, the ST and the TT in order to quantify the selection effects acting on the considered samples and their role on the correlations found.

Our main results are as follows.

(i) *Long GRBs* detected by GBM follow the same $E_{\rm peak}^{\rm obs}$–F and $E_{\rm peak}^{\rm obs}$–P correlations defined by BATSE GRBs (Fig. 2). We computed the instrumental selection effects of GBM – as already done for BATSE (G08; N08): the TT and the ST are not responsible for the correlations defined by long GRBs in both planes (see Fig. 2). The GBM spectral extension down to 8 keV with respect to the limit of 30 keV of BATSE allows us to extend the correlations to lower peak energies/fluences. Instead, despite the higher energy threshold of GBM (40 MeV) no long GRB with $E_{\rm peak}^{\rm obs}$ larger than a few MeV is detected according to Harris & Share (1998). This can be due to a real absence of bursts with such high $E_{\rm peak}^{\rm obs}$ or to the fact that they have large fluences, thus being too rare to be detected during less than 2 years of GBM observations.

We conclude that long GRBs detected by GBM confirm what was found with BATSE bursts, in particular that they follow a correlation both in the $E_{\rm peak}^{\rm obs}$–F and in the $E_{\rm peak}^{\rm obs}$–P plane. Moreover, the fraction of bursts detected by GBM that are outliers at more than 3σ with respect to the $E_{\rm peak}$–$E_{\rm iso}$ correlation is $\sim$3 per cent, to be compared with the 6 per cent of outliers found (N08) in the BATSE sample. In contrast, there are no outliers (at more than 3σ) of the $E_{\rm peak}$–$L_{\rm iso}$ correlation among GBM long GRBs.

(ii) *Short GRBs* detected by GBM populate a different region in the $E_{\rm peak}^{\rm obs}$–F plane with respect to long events, the former having larger peak energies and lower fluences compared to the latter. This is consistent with what is found by BATSE and confirms that short GRBs do not follow the 'Amati' correlation but they can be still consistent with the 'Yonetoku' correlation defined by long events.

The GBM population of long and short bursts with spectral information is large enough to allow a statistical comparison with the BATSE results. For long bursts, we considered the fluence distribution of BATSE bursts, and we compared it to those derived by N11 for GBM bursts. We also compared the spectral properties for selected samples of GBM and BATSE bursts with well-defined $E_{\rm peak}^{\rm obs}$ derived from the spectral analysis. Two different samples of BATSE bursts are available in the literature, based on complementary fluence selection criteria. We call them faint and bright BATSE samples. We then selected from the catalogue of N11 two subsamples of GBM bursts based on the same fluence criteria applied to the BATSE samples (i.e. $10^{-6} < F < 2 \times 10^{-5}$ erg cm^{-2} for the faint GBM sample and $F > 2 \times 10^{-5}$ erg cm^{-2} for the bright GBM sample).

The $E_{\rm peak}^{\rm obs}$ distributions derived from the two instruments are quite similar (Fig. 3 and Table 1). Despite its larger energy range, the GBM extends the $E_{\rm peak}^{\rm obs}$ distribution of long bursts only at low energies with respect to BATSE. The α distribution, instead, reveals some difference for the sample of bright bursts: BATSE bursts have on average a softer low-energy photon index ($\langle\alpha_{\rm GBM}\rangle = -0.9$ and $\langle\alpha_{\rm BATSE}\rangle = -1.1$, KS probability $= 7 \times 10^{-3}$). However, this difference is almost totally due to the presence (in the K06 sample of bright BATSE bursts) of GRBs modelled by an SBPL function. As noted by K06, this model gives a low-energy spectral index systematically softer with respect to COMP and Band models. By excluding these events, the α distribution of bright BATSE bursts is centred around $\langle\alpha_{\rm BATSE}\rangle = -1.00$ and the KS probability with the GBM is 0.46.

Also for GBM short bursts we can draw some conclusions about their spectral properties, even if we warn that the sample of short GBM bursts comprises a quite small number of events. Their $E_{\rm peak}^{\rm obs}$ distribution is shifted towards higher energies compared both with long bursts from the same instrument and with short bursts seen by BATSE. The lack of low-energy $E_{\rm peak}^{\rm obs}$ (below $\sim$200 keV) can be accounted for by the ST we derived for the GBM instrument (see Fig. 2). This hypothesis is supported by the fact that among the population of short GBM bursts there are 44 events fitted with a curved model (i.e. with $E_{\rm peak}^{\rm obs}$ determined) but there exists a large fraction of short bursts (29) whose spectrum is fitted with a single PL. The BATSE sample shows that a fraction of the events with low $E_{\rm peak}^{\rm obs}$ lies above the ST GBM curve and they have sufficient fluence to measure $E_{\rm peak}^{\rm obs}$. Their lack in the GBM sample suggests that they are rare and, due to the still small size of the sample of short GBM GRBs, they may not yet have been observed by *Fermi*. On the other hand, the larger energy coverage allows the detection of $E_{\rm peak}^{\rm obs}$ up to $\sim$4 MeV. GBM data confirm that short bursts have on average a harder α compared with long bursts ($\langle\alpha_{\rm GBM,short}\rangle \sim -0.59$), as already found in the BATSE sample by G09.

The comparison of short and a representative sample of long BATSE GRBs (selected with a similar peak flux threshold) led G09 to conclude that their main spectral diversity is due to a harder low-energy spectral index in short bursts while their $E_{\rm peak}^{\rm obs}$ of BATSE is similarly distributed. GBM bursts provide the opportunity of re-examining this result for the population of short and long GRBs detected by the GBM and also comparing their spectral properties with those of the BATSE ones. We find the following.

(i) $E_{\rm peak}^{\rm obs}$ of short GBM bursts is larger and α smaller that those of long ones, indicating that short events are harder, in terms of both their peak energy and low-energy spectral index.

(ii) A comparison between GBM and BATSE short bursts reveals that they have similar α while the $E_{\rm peak}^{\rm obs}$ of short GBM bursts is larger than that of short BATSE events (see Fig. 2, bottom-left panel). This information is allowed by the higher energies which can be detected by the GBM. Moreover, the different $E_{\rm peak}^{\rm obs}$ distribution of BATSE and GBM short bursts is affected by the lower sensitivity of the GBM instrument, which misses short bursts at low fluences (and therefore low $E_{\rm peak}^{\rm obs}$).

(iii) GBM and BATSE long bursts have a similar $E_{\rm peak}^{\rm obs}$ while GBM events tend to have a harder low-energy spectral index (Fig. 4).

Fig. 8 shows a schematic representation of the current information about the distribution of short and long bursts in the $E_{\rm peak}^{\rm obs}$–F and $E_{\rm peak}^{\rm obs}$–P planes. With respect to BATSE, the GBM reveals that long bursts extend to lower $E_{\rm peak}^{\rm obs}$, consistent with what was previously found with other instruments (mainly *Hete-II* and *Swift*).

Despite the high-energy sensitivity, also the $E_{\rm peak}^{\rm obs}$ distribution of GBM long events extends only up to $\sim$1 MeV (Harris & Share 1998). The situation is different for short GRBs whose $E_{\rm peak}^{\rm obs}$ reach up to $\sim$4 MeV in the present sample. These high $E_{\rm peak}^{\rm obs}$ were not detectable by BATSE, whose sensitivity drops at $\sim$1 MeV (upper horizontal dashed line in Fig. 8). Therefore, the GBM shows that short GRBs have larger $E_{\rm peak}^{\rm obs}$ with respect to long ones, contrary to what is found with BATSE (G09).

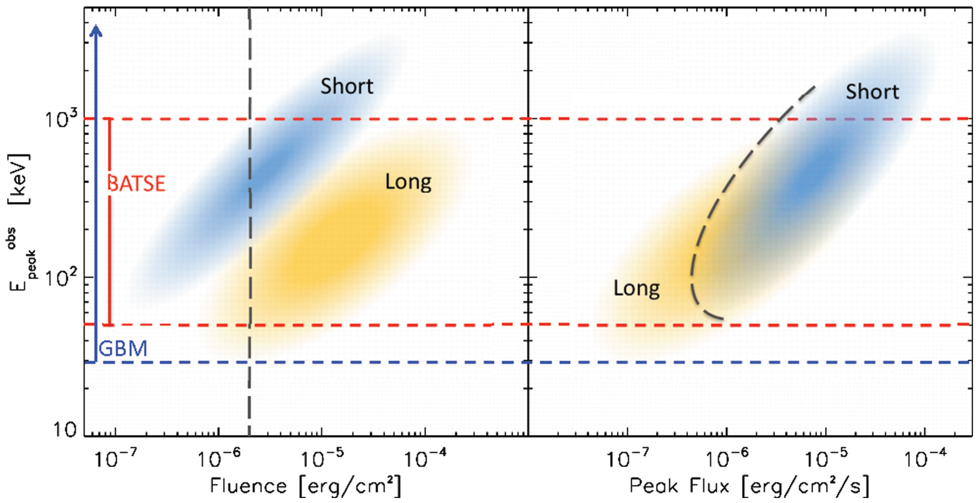

Figure 8. Schematic view of the distribution of long and short GRBs in the $E_{\rm peak}^{\rm obs}$–F and $E_{\rm peak}^{\rm obs}$–P planes. The horizontal dashed line at ∼30 keV represents the lower limit for the GBM instrument: the simulations performed in this work show that $E_{\rm peak}^{\rm obs}$ can be hardly determined below this value. For the BATSE instrument this limit corresponds to ∼50 keV. The upper limit for BATSE is at ∼1 MeV, while for the GBM there is no upper limit in this plane. The vertical dashed line (left-hand panel) shows an example of fluence selection, while the dashed curve (right-hand panel) refers to the photon flux selection criterion adopted by G09.

When comparing the $E_{\rm peak}^{\rm obs}$ distributions of short and long bursts, different conclusions can be drawn, according to the selection criterion of the samples. The left-hand panel in Fig. 8 shows that a given cut in fluence (represented by the vertical dashed line) would result in different $E_{\rm peak}^{\rm obs}$ distributions between short and long bursts, resulting from their different location in the $E_{\rm peak}^{\rm obs}$–F plane. The right-hand panel in Fig. 8 illustrates, instead, what happens for a selection in *photon flux*. This translates into a curve in *energy flux*: the dashed curve represents the cut applied by G09 to select both short and long bursts, corresponding to a photon flux larger than 3 photons cm^{-2} s^{-1}. This criterion applied to BATSE bursts produces similar $E_{\rm peak}^{\rm obs}$ distributions of long and short events, as indeed found by G09. The very same criterion applied to GBM bursts results, instead, in different distributions, since short bursts can have very high $E_{\rm peak}^{\rm obs}$ values, not detected in the sample of long bursts.

ACKNOWLEDGMENTS

We thank Y. Kaneko for private communications on the BATSE bright sample spectral results. This research has made use of data obtained through the high-energy Astrophysics Science Archive Research Center Online Service, provided by the NASA/Goddard Space Flight Center. This work has been partly supported by ASI grant I/088/06/0. LN thanks the Osservatorio Astronomico di Brera for kind hospitality during the completion of this work.

REFERENCES

Amati L. et al., 2002, A&A, 390, 81
Band D., 2003, ApJ, 588, 945
Band D. L., 2006, in Holt S. S., Gehrels N., Nousek J. A., eds, AIP Conf. Ser., Vol. 836, Gamma-Ray Bursts in the *Swift* Era. Am. Inst. Phys., New York, p. 704
Band D. L., Preece R. D., 2005, ApJ, 627, 319
Band D. et al., 1993, ApJ, 413, 281
Firmani C. et al., 2009, MNRAS, 393, 1209
Ghirlanda G., Ghisellini G., Lazzati D., 2004a, ApJ, 616, 331
Ghirlanda G., Ghisellini G., Lazzati D., Firmani C., 2004b, ApJ, 613, L13
Ghirlanda G., Nava L., Ghisellini G., Firmani C., Cabrera J. I., 2008, MNRAS, 387, 319(G08)
Ghirlanda G., Nava L., Ghisellini G., Celotti A., Firmani C., 2009, A&A, 496, 585(G09)
Ghirlanda G., Nava L., Ghisellini G., 2010a, A&A, 511, 43
Ghirlanda G., Nava L., Ghisellini G., Burlon D., 2010b, MNRAS, 510, L7
Guiriec S. et al., 2010, ApJ, 725, 225
Harris M. J., Share G. H., 1998, ApJ, 494, 724
Kaneko Y. et al., 2006, ApJS, 166, 298 (K06)
Kippen R. M., Woods P. M., Heise J., in't Zand J. J. M., Briggs M. S., Preece R. D., 2003, in Ricker G. R., Vanderspek R. K., eds, AIP Conf. Ser. Vol. 662, Gamma-Ray Burst and Afterglow Astronomy 2001. Am. Inst. Phys., New York, p. 244
Krimm H. A. et al., 2009, ApJ, 704, 1405
Lloyd N. M., Petrosian V., Mallozzi R. S., 2000, ApJ, 534, 227
Meegan C. et al., 2009, ApJ, 702, 791
Nakar E., 2007, Phys. Rev., 442, 166
Nakar E., Piran T., 2005, MNRAS, 360, L73
Nava L., Ghirlanda G., Ghisellini G., Firmani C., 2008, MNRAS, 391, 639 (N08)
Nava L., Ghirlanda G., Ghisellini G., Celotti A., 2011, A&A, 530, 21 (N11)
Paciesas W. S., Briggs M. S., Preece R. D., Mallozzi R. S., 2003, in Ricker G. R., Vanderspek R. K., eds, AIP Conf. Ser. Vol. 662, Gamma-Ray Burst and Afterglow Astronomy 2001. Am. Inst. Phys., New York, p. 248
Preece R. D. et al., 2000, ApJS, 126, 19
Sakamoto T., Hullinger D., Sato G., 2008, ApJ, 679, 570
Yonetoku D. et al., 2004, ApJ, 609, 935

This paper has been typeset from a TEX/LATEX file prepared by the author.